

Comparison of Integrated Water Vapor from GNSS and radiosounding at four GRUAN stations

Javier Vaquero-Martínez¹, Manuel Antón

Departamento de Física, Universidad de Extremadura, Badajoz (Spain)

Instituto Universitario de Investigación del Agua, Cambio Climático y Sostenibilidad (IACYS), Universidad de Extremadura, Badajoz (Spain)

José Pablo Ortiz de Galisteo

Agencia Estatal de Meteorología (AEMET), Valladolid (Spain)

Grupo de Óptica Atmosférica, Universidad de Valladolid, Valladolid (Spain)

Roberto Román, Victoria E. Cachorro, David Mateos

Grupo de Óptica Atmosférica, Universidad de Valladolid, Valladolid (Spain)

Abstract

Integrated water vapor (IWV) data from Global Navigation Satellite Systems (GNSS) and radiosounding (RS) are compared over four sites (Lindenberg, Ny-Alesund, Lauder and Sodankyla), which are part of the Global Climate Observing System (GCOS) Reference Upper Air Network (GRUAN). Both datasets show an excellent agreement, with a high degree of correlation (R^2 over 0.98). Dependences of GNSS-RS differences on several variables are studied in detail. Mean bias error (MBE) and standard deviation (SD) increase with IWV, but in relative term, these variables decrease as IWV increases. The dependence on solar zenith angle (SZA) is partially related to the distribution of IWV with SZA, but the increase of SD for low SZA could be associated with errors in the humidity sensor. Large surface pressures worsen performance, which could be due to the fact that low IWV is typically present in high pressure situations. Cloud cover shows a weak influence on the mentioned MBE and SD.

¹javier_vm@unex.es

The horizontal displacement of radiosondes generally causes SD to increase and MBE to decrease (increase without sign), as it could be expected. The results point out that GNSS measurements are useful to analyze performance to other instruments measuring IWV.

1. Introduction

Water vapor has a paramount relevance in the climate system, since it is acknowledged as the most important atmospheric greenhouse gas, and despite of not being directly involved in global warming, it causes a positive radiative feedback on climate system (Colman, 2003, 2015). It also plays a fundamental role in energy transport, evaporating at low latitudes, and being transported to higher latitudes where it condensates, releasing high amounts of latent heat (Myhre et al., 2013).

Integrated water vapor (IWV) is the variable commonly used to study the atmospheric water vapor. IWV is a magnitude equivalent to condensing all the water vapor in the atmospheric vertical column and measuring the height that it would reach if contained in a vessel of unit cross section; being its units those of superficial density (g mm^{-2}) or length (mm).

However, understanding of water vapor effects on climate still needs improving because of the high variability of this gas, both spatially and temporally. It is therefore necessary to retrieve quality water vapor data. Radiosounding (RS) is one of the more precise and direct ways to measure water vapor profiles, and from them IWV data, despite its limitation of temporal resolution (typically one or two launches per day). RS is therefore established as a reference to validate other instruments (du Piesanie et al., 2013; Ohtani & Naito, 2000; Antón et al., 2015). However, it still has some sources of errors as explained in Wang & Zhang (2008) and Dirksen et al. (2014), most of them due to the problem of changes in the radiosonde models and errors in the humidity sensor related to heating by solar radiation.

Moreover, Global Navigation Satellite Systems (GNSS) meteorology is a

relatively recent technique that can be used to derive IWV data (Bevis et al., 1992). GNSS measurements have some advantages: all-weather availability, high temporal resolution (5 min to 2 hourly), high accuracy (less than 3 mm in IWV) and long-term stability. Hence, GNSS data are also used as reference to validate other instruments (Köpken, 2001; Prasad & Singh, 2009; Rama Varma Raja et al., 2008; Román et al., 2015; Vaquero-Martínez et al., 2017a,b, 2018), but as the recent technique that it is, GNSS meteorology still needs validation and assessment of quality in different parts of the Globe.

The Global Climate Observing System (GCOS) Reference Upper-Air Network (GRUAN) has recognized the need of having redundant water vapor measurements in order to improve their quality (GRUAN, 2007). Hence, GRUAN stations that already measure water vapor with RS are being equipped with GNSS receivers and a GRUAN GNSS water vapor product is being developed (WMO, 2008).

The main goal of this study is to analyze the possible errors of the new GNSS IWV products in order to assess their use for other purposes, allowing an improvement in temporal resolution as compared with traditional RS. This way, in this article compare the IWV from GNSS against IWV from RS at the four GRUAN stations with both RS and GNSS water vapor data currently available, and analyze the causes of the differences.

This article is organized as follows: Section 2 describes the different datasets used and their characteristics, and the methodology used in this work. Section 3 includes the results and its discussion, validating the GNSS retrieval performed by the authors for comparison purposes, and analyzing the comparison results. Section 4 summarizes the main conclusions.

2. Material and methods

2.1. IWV from GRUAN GNSS

GNSS consists of a series of satellites that communicate through L-band microwave radiation with receivers, mainly in order to estimate these receivers'

55 locations. The method to obtain IWV from GNSS measurements is detailed in
 56 Bevis et al. (1992), and briefly explained in the following lines.

57 The time spent by the signal in reaching the receiver can be used to calculate
 58 the distance between the satellite and receiver, and taking into account the
 59 position of the satellites, to obtain the receiver's position. However, several
 60 corrections need to be applied, since the signal suffers a series of delays in its
 61 travel to the receiver. There is a particular contribution, the Slant Tropospheric
 62 Delay (STD), that allows IWV calculation. This contribution refers to the delay
 63 that the troposphere causes in the signal, and is referred to the path that the
 64 signal follows. Mapping functions (Niell, 2000; Boehm et al., 2006a,b) can be
 65 applied to obtain the zenithal equivalent of this amount, the Zenith Tropospheric
 66 Delay (ZTD). ZTD is the sum of two contributions, one related to the non-
 67 dipolar contribution of all gases in the troposphere (Zenith Hydrostatic Delay,
 68 ZHD), and another related to the dipolar contribution of water vapor (Zenith
 69 Wet Delay, ZWD) since it is the only compound with dipolar momentum in
 70 the atmosphere. A simple model can estimate accurately ZHD (Saastamoinen,
 71 1972), based on surface pressure. This model is accurate to the submillimeter
 72 region except if that the hydrostatic equilibrium condition does not hold; in
 73 that case errors can reach 1 mm in ZHD. The performance of other models are
 74 similar (Opaluwa et al., 2013). Once ZHD is obtained, ZWD can be estimated
 75 as $ZWD = ZTD - ZHD$.

76 Additionally, another variable is necessary to convert ZWD to IWV, the
 77 water vapor weighted mean temperature in the vertical column (T_m). T_m is
 78 defined as Eq. (1):

$$T_m = \frac{\int \frac{P_v}{T} dz}{\int \frac{P_v}{T^2} dz}, \quad (1)$$

79 where P_v is water vapor partial pressure and T is the temperature, both at
 80 altitude z . T_m is often estimated from surface temperature from meteorological
 81 stations, using empirical fits, or obtained from re-analysis or radiosondes.

82 The product used in this work is developed by GRUAN GNSS (GG) Precip-

itable Water Vapour Task Team. Ground-based GNSS IWV has been identified as a Priority 1 measurement for GRUAN. Therefore, a lot of efforts are being done in the last few years to implement this kind of measurements in GRUAN sites. The sites are Lindenberg (LIN), Sodankylä (SOD), Lauder (LAU) and Ny-Ålesund (NYA). Despite the voluntary nature of GG sites, the GG sites must follow a series of guidelines in order to ensure the quality of GG IWV data. Thus, these sites must be equipped with automatic meteorological stations or there must be a nearby station. The GG locations involved in this work are detailed in Table 1.

GRUAN network provides both ZTD and IWV products for those stations equipped with GNSS. However, sometimes meteorological data (pressure and temperature) are not available and GRUAN provides only ZTD product. The number of days with GG IWV data at every station available for this study is also shown in Table 1. It can be observed that LAU and SOD stations exhibit a reduced number of days with original GG IWV data. To solve this issue and increase the data number, in this work, GRUAN radiosonde meteorological data (T_m and surface pressure) are used to obtain a new IWV product from GG ZTD data (obtained by authors for comparison purposes only). This new product, developed for comparison purposes, is named in this work as “Re-calculated GG IWV product”, while the GNSS IWV product retrieved directly from GRUAN have been named as “Original GG IWV product”. Table 1 shows the number of available days with this re-calculated GG IWV product. It must be noted the notable increase of available days, particularly for LAU and SOD sites. Some restrictions have been applied to ensure data quality:

- Resulting values of IWV must make sense ($0 \text{ mm} < \text{IWV} < 100 \text{ mm}$).
- Mean weighted temperature must be lower than 500 K and positive.

2.2. Radiosoundings from GRUAN network.

GRUAN network provides radiosonde data for 28 sites. We have considered those sites that also have a nearby GNSS product from GRUAN. Table 2 shows

Table 1: Location of the GNSS stations and days with IWV and ZTD data available.

Site	Corresponding RS site	Latitude (°N)	Longitude (°E)	Altitude (m)	Days with IWV data	Days with ZTD data
ldb0	LIN	52.124	14.070	0.002	2143	2164
ldb2	LIN	52.123	14.072	0.160	138	148
ldr2	LAU	-45.022	169.410	0.380	41	98
nya1	NYA	78.555	11.515	0.084	1873	1898
nya2	NYA	78.555	11.513	0.082	0	27
nyal	NYA	78.555	11.521	0.082	0	0
soda	SOD	67.251	26.232	0.300	36	1402
sodf	SOD	67.216	26.375	0.213	0	1

Table 2: Location of RS stations, distance to GNSS sites, and coincident period for both instruments.

Site	Latitude (°N)	Longitude (°E)	Altitude (m)	Distance (km)	Coincident period
LIN	52.210	14.120	112	10.2	12/11/2012 to 04/15/2015
LAU	-45.050	169.680	370	21.5	06/08/2005 to 01/22/2018
SOD	67.370	26.630	179	21.6	05/21/2006 to 05/02/2017
NYA	78.923	11.923	16	42.1	05/15/2007 to 01/10/2018

the locations of the four sites considered in this work.

Typically the radiosonde launches are at specific hours. LIN typically has 4 launches a day (00, 06, 12, 18 h), while NYA’s sondes are typically launched at 12h, and some launches at other hours, specially at 00, 06, and 18 h. Sondes at SOD are launched at 00 and 12 h (some others at different hours), and at LAU at different hours (approximately one launch per week).

The radiosondes that provide the data in this work are Vaisala RS92. The RS92 model is equipped with a wire-like capacitive temperature sensor (“thermocap”); two polymer capacitive moisture sensor (“humicap”), a silicon-based pressure sensor and a GPS receiver. More detailed information about the processing of the data retrieved can be found at <https://www.gruan.org/instruments/radiosondes/sonde-models/vaisala-rs92/> or Dirksen et al. (2014). The main error sources that affect the humidity sensor are: daytime solar heating of the Humicaps (introduces a dry bias), sensor time-lag at temperatures below about -40° (this is not a problem in this work) and temperature

127 dependent calibration correction.

128 The GRUAN RS92 product includes data on profiles of pressure, tempera-
129 ture, humidity, relative humidity, water vapor mixing ratio, wind information,
130 frostpoint, short-wave radiation, and associated uncertainties. IWV can be cal-
131 culated by integration of water vapor mixing ratio (WVMR) in pressures as Eq.
132 (2)

$$\text{IWV} = \int_0^{p_s} \text{WVMR} \cdot dp, \quad (2)$$

133 where WVMR is the water vapor mixing ratio, p is the pressure and p_s the
134 surface pressure. In addition, some restrictions have been considered in order
135 to ensure GRUAN data quality:

- 136 • Number of levels must be more than 15.
- 137 • First level must be at height lower than 1 km.
- 138 • Last level must be at height larger than 9 km.
- 139 • Resulting values of IWV must make sense $0 \text{ mm} < \text{IWV} < 100 \text{ mm}$.

140 2.3. Methodology

141 The followed criterion to match the GNSS and RS data require that time
142 differences between RS launch and GNSS measurement must be below 30 min-
143 utes. For the analysis of differences, RS measurements have been considered
144 as reference and two variables have been analyzed, physical difference (GNSS
145 minus RS) and relative difference (difference divided by RS value). The mean
146 of the differences (also known as mean bias error, MBE) and the standard de-
147 viation of the differences (SD) have been calculated. The SD have been used
148 as a measurement of precision and the MBE as measurement of accuracy. The
149 MBE is calculated as Eq. (3)

$$\text{MBE} = \frac{1}{N} \sum_i^N \delta_i, \quad (3)$$

where δ_i are the physical differences (absolute MBE) or the relative differences (relative MBE). Moreover the SD is obtained as Eq. (4)

$$SD = \sqrt{\frac{1}{N-1} \sum_i^N (\delta_i - \bar{\delta})}. \quad (4)$$

In order to study whether these differences depend on other variables or not, the data have been divided into several bins of similar values of these variables for the study of the precision and accuracy of IWV in each bin. It must be noticed that data bins with less than 15 data have been rejected, as not representative.

3. Results and discussion

3.1. Original GG IWV data vs Re-calculated GG IWV data

Figure 1 shows the correlation between the original and re-calculated GG IWV data. In all stations both data-sets exhibit an excellent agreement ($R^2 \sim 0.99$). All stations show negative offsets (except NYA, which is positive), but all are quite small, less than 0.4 mm in all cases. Outliers, like the ones in NYA and LIN (differences of more than 1.5 mm in IWV), are mainly caused by the differences in pressure measurements. However, around 90% of the data pairs differ by less than 0.7 mm.

Therefore, the data-set of GNSS-derived IWV using meteorological data from radiosonde (GNSSRS) represents very well GRUAN's IWV product. In order to have a data-set with the same features, all the data used in this work will come from the GNSS-derived IWV using meteorological data from radiosonde. The advantages of using this data-set are:

1. More data is available (particularly at SOD and LAU stations).
2. Davis "Mean" temperature can be obtained directly from radiosonde.
3. Temporal interpolation is not necessary.

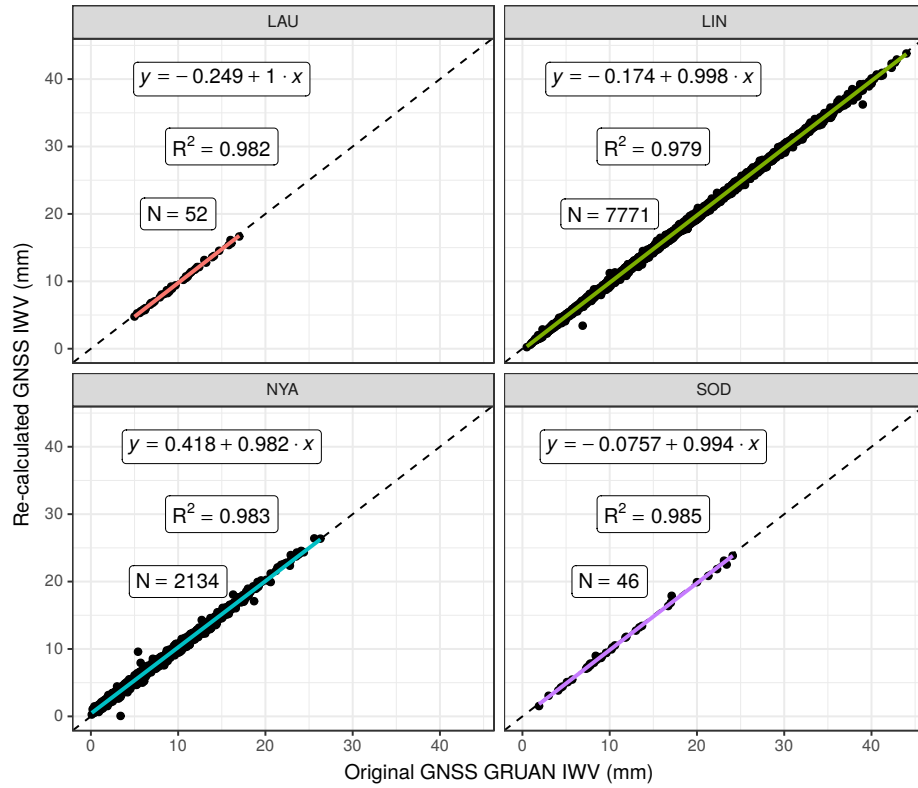


Figure 1: Scatterplots for GNSS-derived IWV from meteorological data provided by GRUAN (x-axis) and meteorological data provided by radiosounding (y-axis) for the four GRUAN stations. Color, continuous lines are regression lines and black, dashed lines are the identity line.

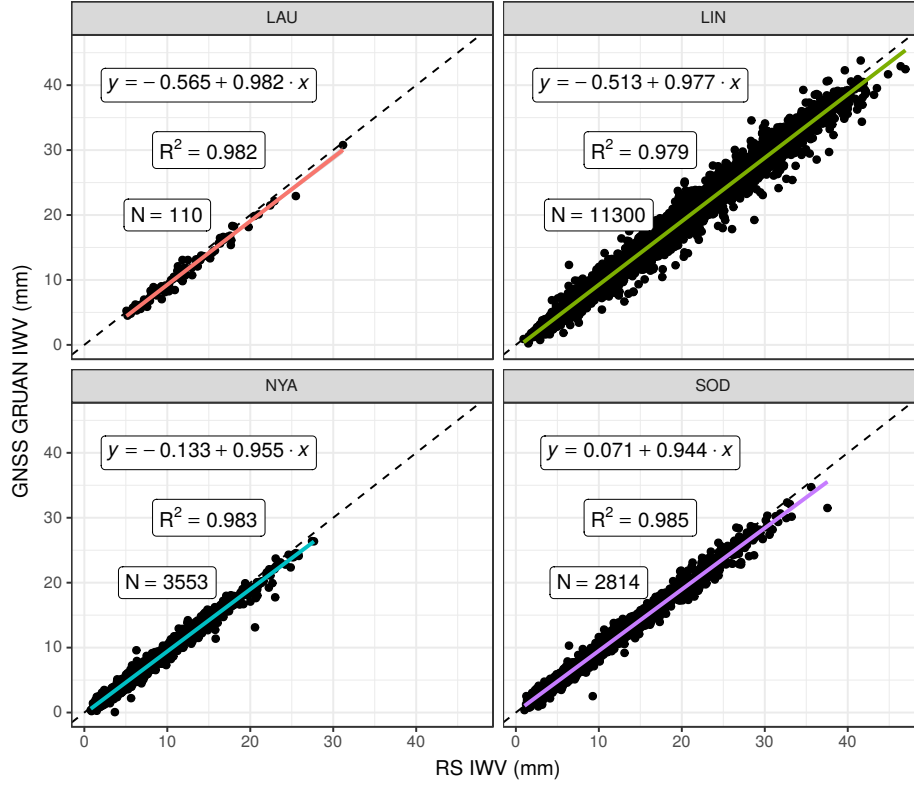


Figure 2: Scatterplots for GNSS IWV data (y-axis) and RS IWV data (x-axis) for the four GRUAN stations. Color, dashed lines are regression lines and black, continuous lines are the identity line.

Needless to say, this is only for comparison purposes, since the radiosonde meteorological data is typically available for at most four times a day, and the GNSS products are available every 15 minutes.

3.2. Comparison between GNSS IWV and RS IWV.

3.2.1. Overall Statistics and regressions.

Table 3 shows a summary of the statistics of the differences between IWV from GNSS and RS. MBE values are over -0.9 mm for all stations, being closer to zero for NYA and SOD (around 0.5 mm). SD values are around $0.6 - 1$ mm. Median and MBE values are similar, which indicates that the

Table 3: Statistics of the differences GNSS IWV - RS IWV (all in mm, except slope and R^2 , which are unitless). MABE is mean absolute bias error, MEDIAN is the median of the differences, IQR is the inter-quartile range of the difference and N the number of data-points.

Site	MBE	SD	MABE	MEDIAN	IQR	N
LAU	-0.767	0.672	0.855	-0.753	0.658	109
LIN	-0.874	1.099	1.094	-0.833	1.150	7837
NYA	-0.492	0.614	0.600	-0.449	0.712	2164
SOD	-0.516	0.830	0.726	-0.435	0.957	2118

183 differences distributions are most likely normal. Figure 2 shows the regression
184 lines. Both data-sets are in agreement with R^2 around 0.98.

185 The differences GNSS-RS and relative differences are analyzed in this section
186 in order to find dependence on different variables. The differences are distributed
187 into bins of similar values of the variable analyzed, and the evolution of MBE
188 and SD over the different bins is analyzed. It must be noticed that the data bins
189 with less than 15 data are not shown, as they are not considered representative.

190 3.2.2. Dependence of GNSS-RS differences on IWV

191 The available data-set have been divided into bins of 5 mm. All stations have
192 a very similar behavior with respect to IWV. The relative MBE in Figure 3 (top)
193 shows that there is a dry bias (around 5%) that decreases in absolute value with
194 IWV. However, for SOD first bin is closer to zero ($\sim 2.5\%$) than the rest of the
195 bins ($\sim 5\%$) of SOD. Absolute MBE (not shown) typically increases in absolute
196 value with IWV, ranging from less than -1 mm up to -2 or -2.5 mm. Such
197 small range explains the behaviour of relative MBE: absolute differences do not
198 change much, but the reference IWV does, thus the relative value decrease (in
199 absolute value) as IWV increases.

200 Regarding precision (see Figure 3, bottom), relative SD, decrease as IWV
201 increases, reaching a minimum of around 5 % in all cases for IWV above 15 mm.

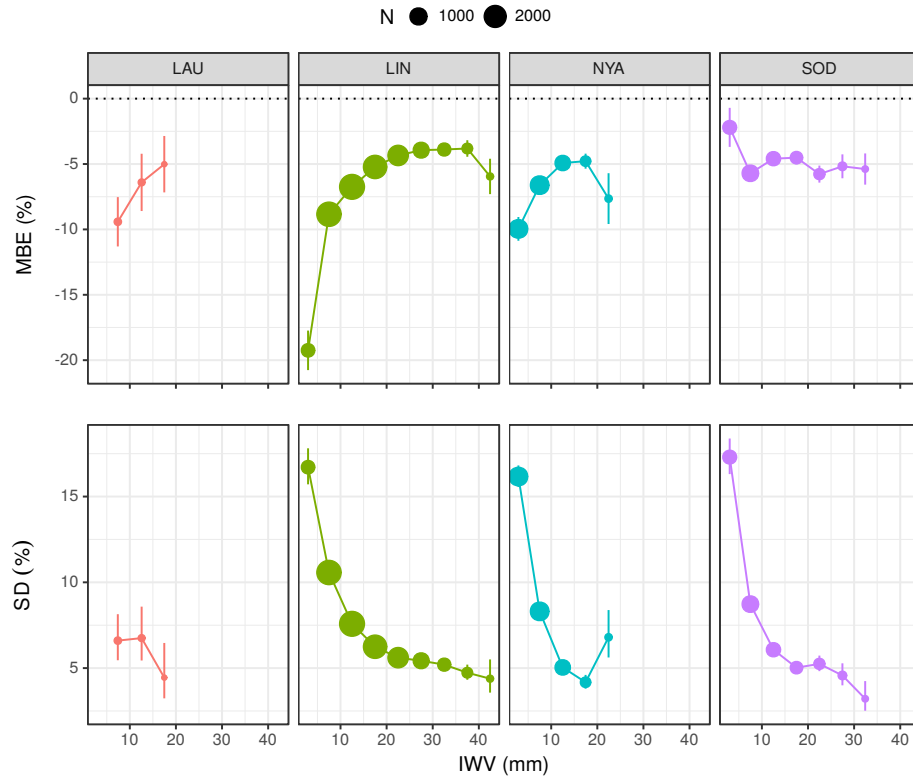


Figure 3: MBE (top) and SD (bottom) of GNSS-RS differences (%) with respect to IWV from RS for the four GRUAN stations.

202 Despite the different ranges of IWV and number of data of each station, the
 203 relative SD is very similar in the lowest bin, between 15 – 17 %). A similar
 204 interpretation to that of the MBE is appropriate here: SD in absolute terms
 205 increases with IWV, but in a range (0.5 – 2 mm) that is quite smaller than the
 206 range of IWV itself (0 – 40 mm), and therefore relative SD tends to decrease
 207 with increasing IWV. Unfortunately, LAU available data does not show a wide
 208 range of IWV, so it is difficult to interpret the results, but they are compatible
 209 with those observed in the rest of sites, with values around 5 – 7 % in the
 210 range of 5 – 20 mm. A similar behaviour was observed in other comparisons
 211 between GNSS and satellite products (Román et al., 2015; Vaquero-Martínez
 212 et al., 2017a,b, 2018) and between RS and satellite products (Antón et al., 2015).
 213 Correlation coefficient R decreases as IWV increases (not shown), from values
 214 over 0.8 for low IWV to values below 0.7 for IWV above 30 mm.

215 *3.2.3. Dependence of GNSS-RS differences on SZA*

216 Differences related to SZA could be due to errors in radiosonde sensors (es-
 217 pecially humidity sensor, which is affected by solar radiation), as stated in Wang
 218 & Zhang (2008) and Dirksen et al. (2014). Figure 4 (top) shows relative MBE
 219 of every 5° bins. It must be noticed that LAU does not have bins with enough
 220 (more than 15) data, so its results are not considered.

221 Although there are some differences between stations, relative MBE gen-
 222 erally worsens as SZA increases. LIN shows a sharp increase at $SZA = 90^\circ$
 223 (sunrise and sunset), while worsening of MBE with SZA is more monotonous
 224 at SOD and NYA, with some increase from 110° . These behaviours are quite
 225 related to typical values of IWV for those SZA bins, especially at LIN: low SZA
 226 causes higher temperatures, which causes the atmosphere to accept more water
 227 vapor and therefore causes IWV to increase. The distribution of IWV with
 228 SZA was checked, confirming this hypothesis. Also, an interesting feature at
 229 LIN IWV was found: SZA increases rapidly around 90° and decreases for SZA
 230 above that value. As NYA and SOD are Arctic stations, the influence of SZA
 231 is not so marked. Values are typically between 5 and 10 %. GOME-2 water

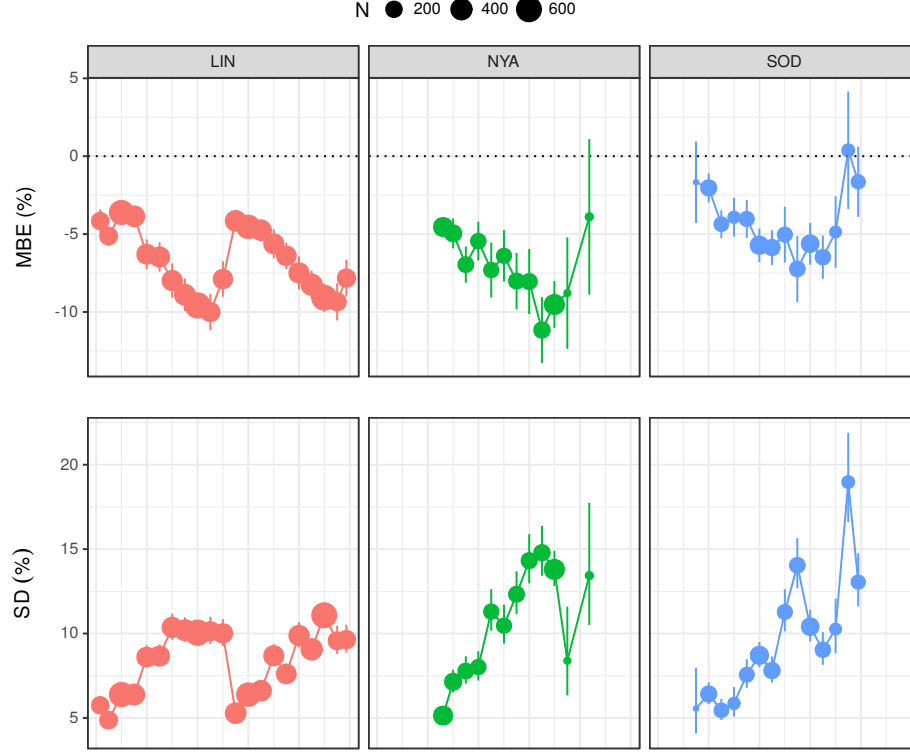


Figure 4: MBE (top) and SD (bottom) of GNSS-RS differences (%) with respect to SZA for three GRUAN stations.

vapor product exhibits a similar behavior, as shown in Antón et al. (2015), but the sign of MBE is positive in that case. Differences between day and night are not important, although in Wang & Zhang (2008) Vaisala RS92 showed a worse performance at day than at night.

In relative terms, as Figure 4 (bottom) reveals, SD increases with SZA. At nighttime, relative SD is higher and more stable, and at daytime, it is lower and has a increasing tendency with SZA. Minimum relative SD for all stations is around 5%, but the maximum differs (10% for LIN, 15% for NYA, and 20% for SOD). This behaviour can be partially due to the observed increase in relative SD for low IWV, with a similar argument to the one provided for relative MBE in this section. In absolute terms (not shown), SD decreases with SZA, which is

243 consistent with this argument, but it could also be related to the fact that at low
 244 SZA the radiosondes humidity sensor can be affected by solar radiation (Dirksen
 245 et al., 2014; Wang & Zhang, 2008) and partly because of the typically higher
 246 IWV values at low SZA. Several satellite product showed similar behaviour (but
 247 with less precision) (Vaquero-Martínez et al., 2018).

248 In this subsection, it is also analyzed the seasonal dependence of GNSS-RS
 249 differences. SZA and IWV both have annual cycles, which cause the MBE and
 250 SD of the differences between IWV from GNSS and RS to have a seasonal de-
 251 pendence as well. LIN and NYA exhibit (not shown) slightly worse relative
 252 MBE in winter (low IWV) than in summer, while SOD (not shown) has worse
 253 relative MBE at summer (higher IWV). Relative SD in LIN, NYA and SOD
 254 are smaller at summer (low SZA) than in winter. The hypothesis that seasonal
 255 dependence on water vapor products performance is mainly affected by depen-
 256 dences on IWV and SZA is also proposed in other works where satellite products
 257 are compared with GNSS ground-based measurements (Vaquero-Martínez et al.,
 258 2017a,b, 2018).

259 3.2.4. *Dependence on pressure*

260 Surface pressure also affects to the GNSS-RS differences. Figure 5 (top)
 261 shows the MBE each 5 hPa bins. Relative MBE increases without sign as
 262 pressure increases. Values are between -15% and 0% approximately. At
 263 high pressures, MBE worsens at a sharper rate. This could be caused by the
 264 distribution of IWV with surface pressure: at high pressure, IWV is smaller,
 265 being the relative MBE higher. Another explanation that could contribute
 266 partially to this behaviour is related to the way that GNSS IWV is retrieved,
 267 since the surface pressure is needed in Saastamoinen’s model (Saastamoinen,
 268 1972).

269 Relative SD, shown in Figure 5) (top), increases with pressure. Values are
 270 between $5 - 10\%$ (LIN), around 10% (NYA) and $5 - 20\%$ (SOD). LAU shows
 271 slight lower values, around 5% but these values are only for low IWV pressure
 272 values. As it also happens with MBE, this behaviour could be partially due to

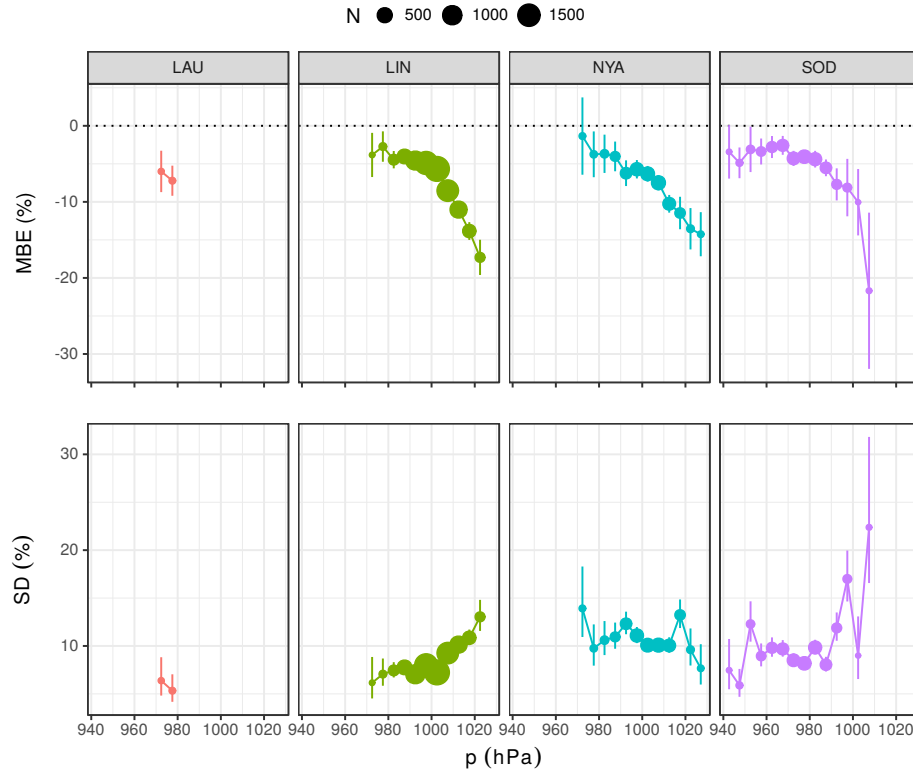


Figure 5: MBE (top) and SD (bottom) of GNSS-RS differences (%) with respect to pressure for the four GRUAN stations.

the distribution of IWV with pressure: lower values of IWV are generally registered at higher values of pressure. SD in absolute terms (not shown) exhibits a maximum (1000 hPa for LIN ,980 hPa for SOD) that is coincident with a maximum in typical IWV values.

3.2.5. *Dependence of GNSS-RS differences on cloudiness*

Total cloud cover data have been obtained from Era-Interim Reanalysis (Dee et al., 2011), and co-located to the sites and times of IWV measurements. These data are in the form of cloud fraction (CF), that is to say, a number between 0 (no clouds) and 1 (totally covered) indicating the pixel cloud cover.

Relative MBE, as shown in Figure 6 (top), is above -4% for LIN and SOD, and between -4 and 12% for NYA. LAU only counts with 1 point, positive relative MBE (less than 2%). However, the results do not show any dependence of MBE on CF. MBE in absolute terms does not show any dependence on CF either.

Regarding relative SD, no tendency is observed (see Figure 6 (bottom)). LIN has very stable values around 8% . NYA however, have highly variable values of SD, some around 7% , other more than 12% , with high uncertainties. Nevertheless, SOD exhibits a slight tendency to decrease SD as CF increases, although still with high variability (between 7% and 15%) and uncertainties.

3.2.6. *Dependence on radiosonde horizontal movement.*

Radiosondes usually move horizontally due to winds. This could be a source of error (Seidel et al., 2011), so it must be taken into account. The distance is obtained as the horizontal distance between the first (closest to the ground) and last (furthest from the ground) radiosonde positions. 20 km bins have been used to study the evolution of MBE and SD throughout the distances.

Figure 7 (top) clearly shows that relative MBE is farther from zero as horizontal displacement increases at NYA, but there is no important trend for the other sites. A reason for this could be that NYA site is located in the Island of Spitsbergen, meaning that a displacement can put the radiosonde over the

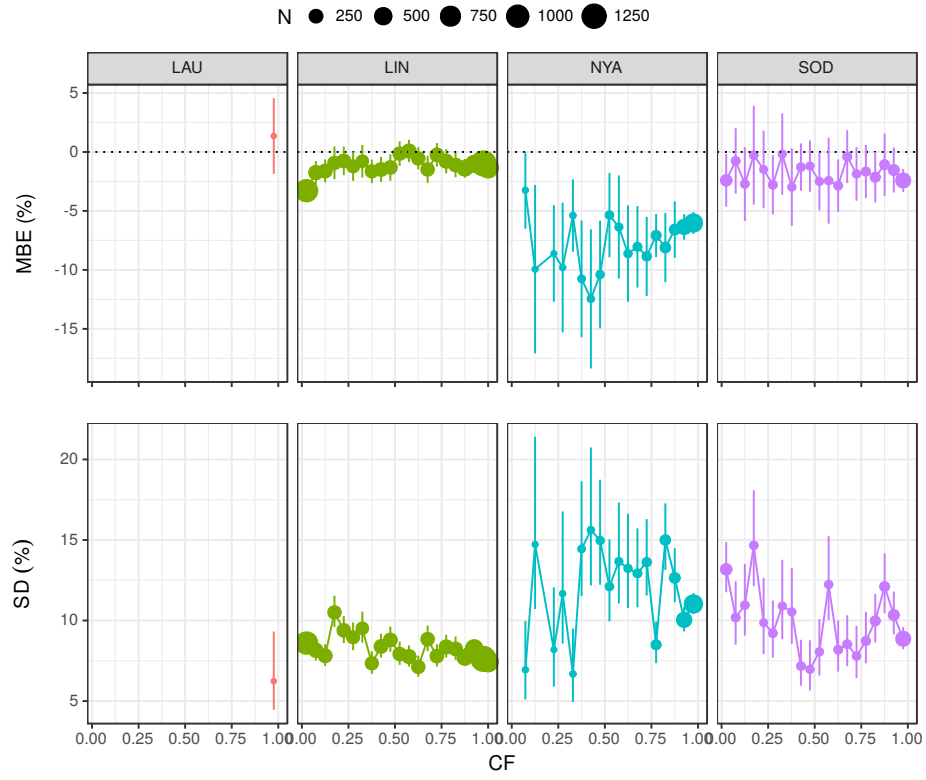


Figure 6: MBE (top) and SD (bottom) of GNSS-RS differences (%) with respect to cloud fraction (CF) for the four GRUAN stations.

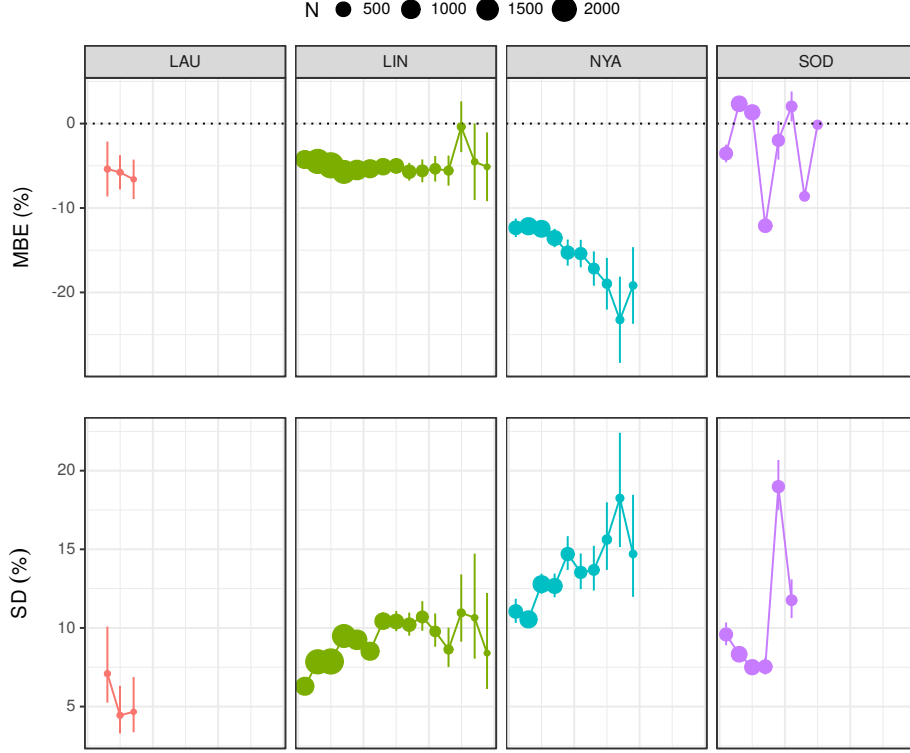


Figure 7: MBE (top) and SD (bottom) of GNSS-RS differences (%) with respect to RS displacement for the four GRUAN stations.

302 sea, where differences with the genuine water vapor vertical profile can be more
 303 important. SOD shows a very high variability, which could be due to inhomogeneous terrain (and thus, humidity) in the vicinity of the site. Relative MBE
 304 changes from -4% to -9% at LIN, and from -10% to -20% at NYA.
 305

306 Figure 7 (bottom) shows the relative SD for several horizontal bins, which
 307 clearly increases as the horizontal displacement increases, which is to be expected. LIN goes from 5% to 15% , NYA from 10% to 20% , and SOD from
 308 0% to 20% . It must be noted the high variability in SOD relative SD values,
 309 which can be caused by the inhomogeneity of the humidity fields in the vicinity
 310 around the site.
 311

312 4. Conclusions

313 Global Climate Observing System (GCOS) Reference Upper Air Network
314 (GRUAN)’s Global Navigation Satellite System (GNSS) and radiosonde (RS)
315 integrated water vapor (IWV) products are in agreement at the sites considered.
316 The regression analysis showed a high correlation ($R^2 > 0.98$) and certain offset
317 that can be due to the spatial separation between GNSS and RS stations. The
318 intercept is positive for all stations except NYA, and the magnitude ranges
319 around 0.1 – 0.2 mm. Values of the standard deviation of the differences (SD)
320 are between 0.6 and 1 mm.

321 The study on dependences of the GNSS-RS differences showed that the mean
322 of the differences (MBE) and SD generally increase (omitting the sign of MBE)
323 with IWV, although relative MBE and SD showed the opposed behavior. Per-
324 formance of RS IWV product was expected to worsen at low solar zenith angle
325 (SZA) because of errors in humidity sensor of radiosondes but this was not ob-
326 served, so corrections are being applied correctly. However, SD does increase
327 at low SZA. Most of the observed dependences on SZA are probably related to
328 the distribution of IWV with SZA (IWV is larger at low SZA, when the tem-
329 peratures are higher). The dependences on SZA and IWV also cause a seasonal
330 dependence.

331 MBE (without sign) and SD exhibits an increase with increasing surface
332 pressure, that can be partially due to the distribution of IWV with pressure
333 (IWV is smaller at high pressures), and partially to errors in the modeling of
334 ZHD through Saastamoinen’s model. However, this is an issue that shall be
335 studied closely in future work. Cloud cover did not show a significant influence
336 on MBE and SD. Regarding dependence on horizontal displacement of radioson-
337 des, the relative MBE and SD show that the performance of RS is poorer when
338 the horizontal displacement is larger, although this seems to be very influence
339 by the characteristics of the site’s vicinity.

340 In summary, the GNSS and RS values are very similar and the dependences
341 on other factors low, but it should be pointed out that it is still very necessary

to have redundant measurements of water vapor in order to improve both the quality of measurements and the sampling of the data. GNSS exhibits two important advantages: first the high temporal resolution, and second the stability against the sky conditions (wind, clouds, etc.), which make GNSS IWV measurement particularly well suited for comparison purposes. However, it must be noticed that the low number of stations do not allow to extract conclusions over the whole range of the variables studied, mainly IWV and SZA.

Acknowledgments

Support from the Junta de Extremadura (Research Group Grants GR15137) is gratefully acknowledged. Work at Universidad de Valladolid is supported by project CMT2015-66742-R. The authors wish to thank the operators at the four observatories (Lindenberg, Lauder, Ny-Ålesund and Sodankylä) for dutifully performing reference radiosoundings and maintenance of GNSS according to the GRUAN standards, as well as GFZ Helmholtz Center Postdam for their procesing of GNSS data products to obtain ZTD and IWV, and acknowledge ERA-Interim data.

References

- Antón, M., Loyola, D., Román, R., & Vömel, H. (2015). Validation of GOME-2/MetOp-A total water vapour column using reference radiosonde data from the GRUAN network. *Atmospheric Measurement Techniques*, 8, 1135–1145. doi:10.5194/amt-8-1135-2015.
- Bevis, M., Businger, S., Herring, T. A., Rocken, C., Anthes, R. A., & Ware, R. H. (1992). GPS Meteorology: Remote Sensing of Atmospheric Water Vapor Using the Global Positioning System. *Journal of Geophysical Research*, 97, 15787–15801. URL: <http://doi.wiley.com/10.1029/92JD01517>. doi:10.1029/92JD01517.

- Boehm, J., Niell, A., Tregoning, P., & Schuh, H. (2006a). Global Mapping Function (GMF): A new empirical mapping function based on numerical weather model data. *Geophysical Research Letters*, *33*, 3–6. doi:10.1029/2005GL025546.
- Boehm, J., Werl, B., & Schuh, H. (2006b). Troposphere mapping functions for GPS and very long baseline interferometry from European Centre for Medium-Range Weather Forecasts operational analysis data. *Journal of Geophysical Research: Solid Earth*, *111*, 1–9. doi:10.1029/2005JB003629.
- Colman, R. (2003). A comparison of climate feedbacks in general circulation models. *Climate Dynamics*, *20*, 865–873. URL: <http://link.springer.com/article/10.1007/s00382-003-0310-z>. doi:10.1007/s00382-003-0310-z. arXiv:183550600013.
- Colman, R. A. (2015). Climate radiative feedbacks and adjustments at the Earth’s surface. *Journal of Geophysical Research: Atmospheres*, *120*, 3173–3182. URL: <http://doi.wiley.com/10.1002/2014JD022896>. doi:10.1002/2014JD022896.
- Dee, D. P., Uppala, S. M., Simmons, A. J., Berrisford, P., Poli, P., Kobayashi, S., Andrae, U., Balmaseda, M. A., Balsamo, G., Bauer, P., Bechtold, P., Beljaars, A. C. M., van de Berg, L., Bidlot, J., Bormann, N., Delsol, C., Dragani, R., Fuentes, M., Geer, A. J., Haimberger, L., Healy, S. B., Hersbach, H., Hólm, E. V., Isaksen, L., Kallberg, P., Köhler, M., Matricardi, M., McNally, A. P., Monge-Sanz, B.M., Morcrette, J.-J., Park, B.-K., Peubey, C., de Rosnay, P., Tavolato, C., Thépaut, J.-N., & Vitart, F. (2011). The ERA-Interim reanalysis: Configuration and performance of the data assimilation system. *Quarterly Journal of the Royal Meteorological Society*, *137*, 553–597. doi:10.1002/qj.828.
- Dirksen, R. J., Sommer, M., Immmler, F. J., Hurst, D. F., Kivi, R., & Vömel, H. (2014). Reference quality upper-air measurements: GRUAN data processing for the Vaisala RS92 radiosonde. *Atmospheric Measurement Tech-*

397 *niques*, 7, 4463–4490. URL: <http://www.atmos-meas-tech.net/7/4463/>
 398 2014/. doi:10.5194/amt-7-4463-2014.

399 du Piesanie, A., Piders, A. J. M., Aben, I., Schrijver, H., Wang, P., & Noël,
 400 S. (2013). Validation of two independent retrievals of SCIAMACHY wa-
 401 ter vapour columns using radiosonde data. *Atmospheric Measurement Tech-*
 402 *niques*, 6, 2925–2940. URL: <http://www.atmos-meas-tech.net/6/2925/>
 403 2013/. doi:10.5194/amt-6-2925-2013.

404 GRUAN (2007). Justification, requirements, siting, and instrumentation
 405 options. URL: [https://www.gruan.org/gruan/editor/documents/gcos/](https://www.gruan.org/gruan/editor/documents/gcos/gcos-112.pdf)
 406 [gcos-112.pdf](https://www.gruan.org/gruan/editor/documents/gcos/gcos-112.pdf).

407 Köpken, C. (2001). Validation of Integrated Water Vapor from Nu-
 408 merical Models Using Ground-Based GPS, SSM/I, and Water Va-
 409 por Radiometer Measurements. *Journal of Applied Meteorology*,
 410 40, 1105–1117. URL: [http://journals.ametsoc.org/doi/abs/10.1175/](http://journals.ametsoc.org/doi/abs/10.1175/1520-0450%282001%29040%3C1105%3AVOIWVF%3E2.0.CO%3B2)
 411 [1520-0450%282001%29040%3C1105%3AVOIWVF%3E2.0.CO%3B2](http://journals.ametsoc.org/doi/abs/10.1175/1520-0450%282001%29040%3C1105%3AVOIWVF%3E2.0.CO%3B2). doi:10.1175/
 412 [1520-0450\(2001\)040<1105:VOIWVF>2.0.CO;2](http://journals.ametsoc.org/doi/abs/10.1175/1520-0450(2001)040<1105:VOIWVF>2.0.CO;2).

413 Myhre, G., Shindell, D., Bréon, F.-M., Collins, W., Fuglestedt, J., Huang, J.,
 414 Koch, D., Lamarque, J.-F., Lee, D., Mendoza, B., Nakajima, T., Robock, A.,
 415 Stephens, G., Takemura, T., & Zhang, H. (2013). Anthropogenic and Natural
 416 Radiative Forcing. In IPCC (Ed.), *Climate Change 2013: The Physical Sci-*
 417 *ence Basis. Contribution of Working Group I to the Fifth Assessment Report*
 418 *of the Intergovernmental Panel on Climate Change* (pp. 659–740). IPCC.
 419 (Ippc ed.).

420 Niell, A. E. (2000). Improved atmospheric mapping functions for
 421 VLBI and GPS. *Earth, Planets and Space*, 52, 699–702. URL:
 422 [http://earth-planets-space.springeropen.com/articles/10.1186/](http://earth-planets-space.springeropen.com/articles/10.1186/BF03352267)
 423 [BF03352267](http://earth-planets-space.springeropen.com/articles/10.1186/BF03352267). doi:10.1186/BF03352267.

424 Ohtani, R., & Naito, I. (2000). Comparisons of GPS-derived precipitable water

425 vapors with radiosonde observations in Japan. *Journal of Geophysical Re-*
426 *search: Atmospheres*, 105, 26917–26929. URL: [http://doi.wiley.com/10.](http://doi.wiley.com/10.1029/2000JD900362)
427 1029/2000JD900362. doi:10.1029/2000JD900362.

428 Opaluwa, Y. D., Adejare, Z. A. T., Abazu, I. C., Adewale, T. O., Odesanmi,
429 A. O., & Okorochoa, V. C. (2013). Comparative Analysis of Five Standard
430 Dry Tropospheric Delay Models for Estimation of Dry Tropospheric Delay
431 in Gns Positioning. *American Journal of Geographic Information System*,
432 (p. 11).

433 Prasad, A. K., & Singh, R. P. (2009). Validation of MODIS Terra,
434 AIRS, NCEP/DOE AMIP-II Reanalysis-2, and AERONET Sun pho-
435 tometer derived integrated precipitable water vapor using ground-based
436 GPS receivers over India. *Journal of Geophysical Research*, 114,
437 D05107. URL: <http://doi.wiley.com/10.1029/2008JD011230>. doi:10.
438 1029/2008JD011230. arXiv:16510847.

439 Rama Varma Raja, M. K., Gutman, S. I., Yoe, J. G., McMillin, L. M., & Zhao,
440 J. (2008). The Validation of AIRS Retrievals of Integrated Precipitable Water
441 Vapor Using Measurements from a Network of Ground-Based GPS Receivers
442 over the Contiguous United States. *Journal of Atmospheric and Oceanic*
443 *Technology*, 25, 416–428. URL: [http://journals.ametsoc.org/doi/abs/](http://journals.ametsoc.org/doi/abs/10.1175/2007JTECHA889.1)
444 10.1175/2007JTECHA889.1. doi:10.1175/2007JTECHA889.1.

445 Román, R., Antón, M., Cachorro, V., Loyola, D., Ortiz de Galisteo,
446 J., de Frutos, A., & Romero-Campos, P. (2015). Comparison of to-
447 tal water vapor column from GOME-2 on MetOp-A against ground-
448 based GPS measurements at the Iberian Peninsula. *Science of The*
449 *Total Environment*, 533, 317–328. URL: [http://linkinghub.elsevier.](http://linkinghub.elsevier.com/retrieve/pii/S0048969715303260)
450 [com/retrieve/pii/S0048969715303260](http://linkinghub.elsevier.com/retrieve/pii/S0048969715303260). doi:10.1016/j.scitotenv.2015.
451 06.124. arXiv:26172599.

452 Saastamoinen, J. (1972). Atmospheric Correction for the Troposphere and
453 Stratosphere in Radio Ranging Satellites. In S. W. Henriksen, A. Mancini, &

454 B. H. Chovitz (Eds.), *Geophysical Monograph Series* (pp. 247–251). American
 455 Geophysical Union. URL: <http://doi.wiley.com/10.1029/GM015p0247>.
 456 doi:10.1029/GM015p0247.

457 Seidel, D. J., Sun, B., Pettey, M., & Reale, A. (2011). Global radiosonde
 458 balloon drift statistics. *Journal of Geophysical Research*, 116. URL: <http://doi.wiley.com/10.1029/2010JD014891>. doi:10.1029/2010JD014891.

460 Vaquero-Martínez, J., Antón, M., Ortiz de Galisteo, J. P., Cachorro, V. E.,
 461 Álvarez-Zapatero, P., Román, R., Loyola, D., Costa, M. J., Wang, H.,
 462 Abad, G. G., & Noël, S. (2018). Inter-comparison of integrated water
 463 vapor from satellite instruments using reference GPS data at the Iberian
 464 Peninsula. *Remote Sensing of Environment*, 204, 729–740. URL: <http://linkinghub.elsevier.com/retrieve/pii/S0034425717304406>. doi:10.
 465 1016/j.rse.2017.09.028.
 466

467 Vaquero-Martínez, J., Antón, M., Ortiz de Galisteo, J. P., Cachorro, V. E.,
 468 Costa, M. J., Román, R., & Bennouna, Y. S. (2017a). Validation of
 469 MODIS integrated water vapor product against reference GPS data at
 470 the Iberian Peninsula. *International Journal of Applied Earth Observation*
 471 *and Geoinformation*, 63, 214–221. URL: <http://linkinghub.elsevier.com/retrieve/pii/S0048969716327176>. doi:10.1016/j.jag.2017.07.008.
 472 arXiv:27988187.
 473

474 Vaquero-Martínez, J., Antón, M., Ortiz de Galisteo, J. P., Cachorro, V. E.,
 475 Wang, H., González Abad, G., Román, R., & Costa, M. J. (2017b). Vali-
 476 dation of integrated water vapor from OMI satellite instrument against ref-
 477 erence GPS data at the Iberian Peninsula. *Science of The Total Environ-*
 478 *ment*, 580, 857–864. URL: [http://linkinghub.elsevier.com/retrieve/](http://linkinghub.elsevier.com/retrieve/pii/S0048969716327176)
 479 [pii/S0048969716327176](http://linkinghub.elsevier.com/retrieve/pii/S0048969716327176). doi:10.1016/j.scitotenv.2016.12.032.

480 Wang, J., & Zhang, L. (2008). Systematic Errors in Global Radiosonde Precip-
 481 itable Water Data from Comparisons with Ground-Based GPS Measurements.

482 *Journal of Climate*, 21, 2218–2238. URL: <http://journals.ametsoc.org/>
483 [doi/abs/10.1175/2007JCLI1944.1](http://journals.ametsoc.org/doi/abs/10.1175/2007JCLI1944.1). doi:10.1175/2007JCLI1944.1.

484 WMO (2008). Report of the GCOS Reference Upper-Air Network Implemen-
485 tation Meeting. URL: [https://www.gruan.org/gruan/editor/documents/](https://www.gruan.org/gruan/editor/documents/gcos/gcos-121.pdf)
486 [gcos/gcos-121.pdf](https://www.gruan.org/gruan/editor/documents/gcos/gcos-121.pdf).